Whole-Body Biodistribution, Radiation Absorbed Dose and Brain SPECT Imaging with Iodine-123-β-CIT in Healthy Human Subjects

John P. Seibyl, Elizabeth Wallace, Eileen O. Smith, Michael Stabin, Ronald M. Baldwin, Sami Zoghbi, Yolanda Zea-Ponce, Y. Gao, W.Y. Zhang, John L. Neumeyer, I. George Zubal, Dennis S. Charney, Paul B. Hoffer and Robert B. Innis

Departments of Psychiatry and Diagnostic Radiology, Yale University School of Medicine, New Haven; and West Haven VA Medical Center, West Haven, Connecticut; Research Biochemicals International, Natick, Massachusetts; and Oak Ridge Institute for Science and Education, Oak Ridge, Tennessee

SPECT imaging with ^{123}I-labeled methyl 3β-(4-iodophenyl)tropane-2β-carboxylate ([^{123}I]β-CIT) in nonhuman primates has shown brain striatal activity, which primarily reflects binding to the dopamine transporter. The biodistribution and calculated radiation-absorbed doses of [^{123}I]β-CIT administered to eight healthy subjects were measured with attention to the accurate determination of organ time-activity data. **Methods:** Whole-body transmission images were obtained with a scanning line source for attenuation correction of the emission images. Following administration of 92.5 ± 22.2 MBq (2.5 ± 0.6 mCi) of [^{123}I]β-CIT, subjects were imaged with a whole-body imager every 30 min for 3 hr, every 60 min for the next 3 hr and at 12, 24 and 48 hr postinjection. Regional body conjugate counts were converted to microcuries of activity, with a calibration factor determined in a separate experiment using a distributed source of ^{123}I. **Results:** The peak brain uptake represented 14% of the injected dose, with 2% of the activity approximately overlying the striatal region. Highest radiation-absorbed doses were to the lung (0.1 mGy/MBq, 0.38 rads/mCi), liver (0.087 mGy/MBq, 0.32 rads/mCi) and lower large intestine (0.053 mGy/MBq, 0.20 rads/mCi). **Conclusions:** Iodine-123-β-CIT is a promising SPECT agent for imaging of the dopamine transporter in humans with favorable dosimetry and high brain uptake.

Key Words: iodine-123-β-CIT; biodistribution; SPECT; monoamine transporter; dosimetry

J Nucl Med 1994; 35:764–770

Monoaminergic neural transmission is partly regulated by the reuptake of a released transmitter by the presynaptic neuron. A neurotransmitter is reincorporated into the cell by monoamine-specific transporters located on the presynaptic neuronal membrane. The critical role of these transporters in regulating dopamine neuronal function makes them of potential interest in several neuropsychiatric disorders, including Parkinson's disease, schizophrenia and psychostimulant abuse (*1–5*).

Recent work established the feasibility of in vivo imaging of brain monamine transporters with ^{123}I-labeled methyl 3β-(4-iodophenyl)tropane-2β-carboxylate ([^{123}I]β-CIT, also designated RTI-55) (*1–3*). In vitro radioligand binding showed that β-CIT has a high affinity for the dopamine (IC_{50} = 1.6 n*M*) and serotonin (IC_{50} = 3.78 n*M*) transporters based on displacement of [^{3}H]CFT and [^{3}H]paroxetine, respectively (*6–10*). Brain SPECT in anesthetized monkeys showed brain uptake of 6%–10% of injected radiotracer with striatal to cerebellar ratios of 7.3 at 5 hr postradioligand administration (*11,12*). These studies suggest [^{123}I]β-CIT has favorable properties for brain SPECT imaging of dopamine and serotonin transporters in humans.

The characterization of human biodistribution and organ radiation burden is a prerequisite to the extension of [^{123}I]β-CIT brain SPECT to central nervous system disease. Biodistribution and dosimetry studies of investigational radiopharmaceuticals have been limited by inaccurate characterization of organ time-activity data because of limited sampling, inadequate attenuation correction or other errors in the quantification of activity. The purposes of the present investigation were (1) to measure the whole-body biodistribution of [^{123}I]β-CIT and calculate the associated radiation-absorbed doses in healthy human subjects with attention to the accurate measurement of source organ activity and (2) to characterize the in vivo human brain distribution of [^{123}I]β-CIT using SPECT.

Received Aug. 27, 1993; revision accepted Dec. 20, 1993.
For correspondence or reprints contact: John P. Seibyl, MD, Psychiatry Service, West Haven VA Medical Center/116A2, 950 Campbell Ave., West Haven, CT 06516.

METHODS

Radiopharmaceutical Preparation and Purity

The radiopharmaceutical [^{123}I]β-CIT was prepared from the corresponding trimethylstannyl precursor and high-radionuclidic purity [^{123}I]NaI (Nordion International, Vancouver, BC, Canada), as previously described (*11*). Radiochemical purity was determined by high-performance liquid chromatography, and specific activity was measured by comparing ultraviolet absorbance of the labeled product with a standard curve made from authentic β-CIT. The [^{123}I]β-CIT was obtained in an average radiochemical yield of 54.8% ± 10.0% (n = 5, mean ± s.e.m.), radiochemical purity of 97.6% ± 1.0% and specific activity >5000 Ci/mmole. Sterility was confirmed by lack of bacterial growth in two media: trypticase and fluid thioglycollate (*13*). Apyrogenicity was confirmed using the limulus amebocyte lysate test (Endosafe, Charleston, SC).

Subjects

Eight healthy subjects (four men and four women; age range 22.4 ± 3.2 yr; weight range 68.6 ± 10 kg, with these and all subsequent values expressed as mean ± s.d.) were enrolled in the study after providing informed consent. The subjects were free of medical or neuropsychiatric illness on the basis of a screening history by a research psychiatrist, physical examination, serum chemical analysis, complete blood count, thyroid indices and urinalysis. The subjects received oral Lugol's solution (containing 400 mg of potassium iodide) 12 and 2 hr prior to the [^{123}I]β-CIT injection.

Data Acquisition

Whole-body transmission and emission scans were performed on the Strichman model 860 whole-body imager (Medfield, MA). This device is a multicrystal dual-headed scanning system that acquires simultaneous anterior and posterior images. SPECT brain images were obtained 5.5 to 27 hr postinjection of [^{123}I]β-CIT with a head-dedicated annular-ring SPECT camera (Ceraspect, Digital Scintigraphics, Waltham, MA).

Attenuation Correction Scans. A whole-body transmission scan was acquired in each subject prior to the injection of the radiotracer by affixing a line source containing 37 to 74 MBq (1–2 mCi) ^{123}I to the posterior camera head and recording counts from the anterior head. Regions of interest (ROIs) were drawn on whole-body transmission images (brain, lung, heart, liver, stomach/spleen, intestine and bladder) and an off-body region. A transmission factor reflecting the fraction of counts passing through the ROI was calculated in each subject by determining the ratio of the counts/pixel detected over each organ divided by the counts/pixel for a region off the body (i.e., not attenuated). This ratio is equal to $e^{-\mu d}$ where μ is the linear attenuation coefficient in units of reciprocal centimeters and d is the thickness of the attenuating medium in centimeters (*14*). Correction for the attenuation of the conjugate count emission images was done by dividing the geometric mean of the anterior and posterior counts in each ROI by an attenuation factor ($e^{-\mu d/2}$) equal to the square root of the transmission factor. Transmission factors were derived in two subjects using both ^{99m}Tc- and ^{123}I-containing line sources to compare the attenuation of emissions from the two different isotopes.

An additional method of attenuation correction was performed in four subjects. Prior to [^{123}I]β-CIT injection, 4 × 4-cm gauze pads containing 7.4 MBq (200 μCi) of ^{123}I were placed over each subject's head (brain), right thorax (lung), left thorax (heart), right upper quadrant (liver), midabdomen (gastrointestinal tract) and pubis (bladder). A standard pad source was placed on the table adjacent to the subject, anterior and posterior images were acquired, and an attenuation factor was calculated by the following formula:

$$\frac{\sqrt{(\text{anterior} \times \text{posterior counts in body region pad})}}{\sqrt{(\text{anterior} \times \text{posterior counts in off body pad}}} = e^{-\mu d/2}. \quad \text{Eq. 1}$$

These attenuation factors were compared with factors derived using the ^{123}I transmission method by using one-way analysis of variance.

Emission Scans. Whole-body emission scans were performed following the intravenous administration of 92.5 ± 22.2 MBq (2.5 ± 0.6 mCi, range 1.9–3.2 mCi) of [^{123}I]β-CIT. Anterior and posterior emission images were obtained using parallel-hole collimation and a 20% symmetric energy window with a photopeak of 159 keV. Serial whole-body images were obtained every 30 min for 3 hr, then every 60 min for 3 more hr and at 12, 24 and 48 hr postinjection.

Brain SPECT Scan. SPECT brain scans were obtained 5.5 to 27 hr postradiotracer injection in all subjects. One subject was imaged twice, at 7 and 11 hr postinjection. Images were acquired over 15 min with a 20% symmetric energy window centered at 159 keV. They were reconstructed with a Butterworth filter (cutoff = 1 cm, power factor = 10) and displayed as 32 slices of 64 × 64 pixels.

Urine Collections. Urine collections were obtained from six subjects over 48 hr postadministration of radiotracer for the following postinjection intervals: 0–6, 6–12, 12–18, 18–24, 24–36 and 36–48 hr. For each period, three 1-ml urine aliquots were counted in an automatic-well gamma counter (model 8000, Beckman Instruments, Fullerton, CA) and expressed as microcuries per milliliter. The counting efficiency of the system was determined by counting a calibrated source of ^{123}I with similar geometry to that of the samples. Radioactivity measurements were corrected for the physical decay of ^{123}I and multiplied by the urine volume in each sampling time to express the radioactivity in the sample as the percent of injected [^{123}I]β-CIT.

Data Analysis

The geometric mean of anterior and posterior counts was calculated for large ROIs for the following organs: whole brain, striatum, lungs, heart, liver, spleen, bladder and remainder of abdomen (gastrointestinal activity) using software written for the Macintosh computer (Image 1.41, Apple, Cupertino, CA). Regions were placed abutting each other to provide accurate recovery of all the injected activity. Conjugate counts were corrected for regional attenuation by the transmission scan method described earlier. These data were converted to microcuries of activity by application of a conversion factor determined in a separate experiment with a 111-MBq (3 mCi) ^{123}I distributed gauze pad source imaged serially on the Strichman 860 whole-body imaging device over 24 hr. The activity of this source was well below the range for camera deadtime effects. This was checked by decay correcting the serial counts to generate a straight time-activity curve. The slope of the line fit to the geometric mean of the anterior and posterior pad counts plotted against the known millicurie activity provided the conversion factor in units of microcuries per square root of counts squared.

Decay-corrected organ data at each time point were converted to the percent of the injected dose by dividing the organ activity

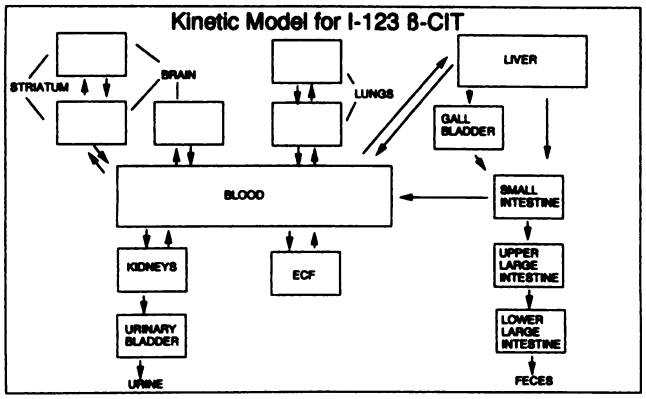

FIGURE 1. Compartmental kinetic model describing biodistribution and excretory pathways for [^{123}I]β-CIT.

by the total injected activity for each subject times 100. The time-to-peak percent dose uptake was determined by taking the single highest point for each organ. The mean and s.d. of the peak percent of the injected dose and the time-to-peak uptake was calculated for each source organ.

Dosimetry calculations were obtained by compartmental modeling of the biodistribution time-activity data (normalized to 100% injected activity). Activity leaving the liver was assumed to clear into the small intestine (70%) or gallbladder (30%). The gallbladder was modeled as filling for 4 hr then clearing for 2 hr into the small intestine with a transfer rate coefficient of 1.8 hr^{-1}. Activity entering the small intestine was assumed to clear to the upper and lower large intestine and feces, according to the International Commission on Radiological Protection gastrointestinal tract model (*15*). Twenty-five percent of the activity entering the small intestine was assumed to be reabsorbed into the blood pool, based on an analysis of the fraction of urinary and gastrointestinal excretion calculated from the total body activity on the last whole-body scan and recovered urine activity. Data for urinary clearance were also fit by the compartmental model. The urinary bladder was assumed to empty every 4.8 hr. Radiation-absorbed doses were calculated using average residence times for all subjects that were estimated from the integration of the time-activity curves for the various compartments in the kinetic model (*16*). The effective dose equivalent, as defined by the International Commission on Radiological Protection, was also calculated (*15*).

Because activity was quantified in the striatum and whole brain, the kinetic model accounted for the activity in the striatum as part of the whole brain (Fig. 1). The absorbed dose to the striatum was estimated by assuming the striatum is a soft-tissue structure composed of two 13.2-g spheres (*17*). All electron energy emitted was assumed to be absorbed within the structure; the photon dose for each sphere was calculated by linearly interpolating between the absorbed fractions for 10- and 20-g spheres following the Medical Internal Radiation Dose Committee's guidelines (*18*). Photon crossfire between the two spheres was neglected.

SPECT brain images were acquired as 32 slices in a 64 × 64 matrix. Transaxial slices were attenuation corrected by placing an ellipse drawn around brain and assuming uniform attenuation (μ = 0.15 cm^{-1}). The four transaxial slices demonstrating the highest striatal uptakes were summed, and a standard ROI template, containing left striatum, right striatum, midbrain and occipital, cortex was applied. The ratios of the activities (expressed as counts per minute per voxel) in the striatum and midbrain to that in the occipital cortex were calculated for the three early scans (5.5–7 hr postinjection) and six later scans (11–27 hr postinjection).

In four subjects, total-brain and striatal counts were determined and converted to megabecquerels using a calibration factor from a cylindrically distributed source phantom of 20-cm diameter filled with an ^{123}I solution using identical windowing and SPECT acquisition parameters. Activities in the total brain and striatum were expressed as percent injected activity for comparison with planar estimates.

RESULTS

Attenuation Correction: Pad Source and Transmission Scan Methods

Comparison of attenuation correction factors derived from the ^{123}I pad sources and the ^{123}I transmission method (Table 1) demonstrated no significant differences in the attenuation factors ($e^{-\mu d/2}$) for brain (F = 3.42, p = 0.09), lung (F = 0.72, p = 0.24), heart (F = 1.70, p = 0.22), intestine (F = 0.28, p = 0.60) or bladder (F = 1.88, p = 0.20). Liver attenuation correction factors obtained by the two methods showed a nonsignificant trend toward difference (F = 4.72, p = 0.06).

Comparison of the transmission factors obtained for organs using ^{123}I- and ^{99m}Tc-containing line sources showed no mean differences in the factors determined in two subjects with ^{99m}Tc compared with ^{123}I in all eight subjects. However, within-subject comparison demonstrated that ^{99m}Tc provided attenuation factors 4%–8% greater for all organs than those from the ^{123}I line source.

TABLE 1
Attenuation Correction Factors ($e^{-\mu d/2}$) Obtained by Transmission Line Source and Emission Pad Source Methods

	Brain	Lung	Heart	Liver	Intestine	Stomach	Bladder	Whole body
^{123}I transmission	0.35	0.46	0.31	0.31	0.30	0.33	0.30	0.48
Mean ± s.d. (n = 8)	0.03	0.04	0.04	0.04	0.04	0.05	0.03	0.04
^{99m}Tc transmission	0.34	0.47	0.31	0.29	0.29	0.33	0.29	0.48
Mean ± s.d. (n = 2)	0.05	0.07	0.06	0.06	0.09	0.04	0.09	0.05
^{123}I pads	0.32	0.49	0.27	0.39	0.29		0.27	
Mean ± s.d. (n = 4)	0.02	0.06	0.05	0.10	0.03		0.03	

TABLE 2
Accuracy of Attenuation and Conversion Factors*

	Whole-body ROI†	Sum of source organ ROI†
Mean % ± s.d. (n = 8)	118.0 10.1	121.0 5.3

*Percent recovery of injected dose for whole-body ROI and summed source organ ROIs

†Images obtained at 3 hr postinjection. Data were corrected for attenuation and decay, converted to microcuries of activity and expressed as the percent of the injected dose.

Recovery of Injected Activity: Accuracy of Attenuation and Conversion Factors

Two different methods were used to estimate the accuracy of the recovery of injected activity (Table 2). The first method summed the ROIs on the 3-hr images, a time after clearance of blood pool activity and before urinary or fecal excretion of injected activity. The presence of significant blood pool activity would underestimate the recovery because ROIs did not include upper and lower extremities. The mean recovery of the decay-corrected percent of the injected dose of the summed ROIs at 3 hr was 121% ± 5% injected dose.

To assess the underestimation of recovery caused by the limited ROIs that covered only the head and torso, the authors drew on each of the eight emission scans obtained at 3 hr a single whole-body ROI that included the head, torso, upper extremities to the elbow and legs to the knees. This ROI was placed on the transmission scan to derive a whole-body attenuation factor (the square root of the fraction of activity passing through the body). This factor was then applied to the counts on the identical whole-body ROI on the emission scan. The attenuation-corrected data were decay corrected, converted to millicuries of activity and expressed as the percent of injected activity. Mean recovery was 118% ± 10% of injected activity, virtually identical to the method summing organ ROIs. The mean 118% recovery was used to correct the time-activity data to 100% injected activity prior to dosimetry calculations.

Biodistribution and Peak Organ Uptake

The decay-corrected organ time-activity curves demonstrated a high initial distribution of tracer to the lungs with subsequent distribution to the liver, intestine and brain (Fig. 2). The peak percents of the injected dose to the lungs, liver, intestine and brain were 75%, 37%, 34% and 14%, respectively. The peak striatal uptake was 2%, with high variability in the time to peak and slow biologic washout of the tracer (Fig. 3).

Radiation Absorbed Dose Estimates

Average residence times for all subjects and radiation-absorbed dose estimates based on these residence times are described in Table 3. The highest absorbed organ doses were to the lungs (0.1 mGy/MBq, 0.38 rads/mCi), liver (0.087 mGy/MBq, 0.32 rads/mCi) and large intestines (0.05 mGy/MBq, 0.2 rads/mCi). The effective dose equivalent was 0.036 mGy/MBq (0.13 rads/mCi). The dose to the striatum was estimated to be 0.26 mGy/MBq (0.96 rads/mCi). Inclusion of the striatal dose estimate as a "remainder" organ in the calculation raised the effective dose equivalent to 0.048 mGy/MBq (0.18 rads/mCi).

Brain SPECT

All subjects demonstrated marked concentration of brain activity in the striatum with relatively low cortical uptake (Fig. 4). The calculated percents of the injected dose for total brain and striatum were in close agreement with the planar imaging data (Table 4), despite differences in the methods of attenuation correction and ROI placement.

The ratios of the striatal-to-occipital and midbrain-to-occipital count density were calculated for visually identified ROIs. The striatal-to-occipital ratio was 5.0 ± 2.3 and 4.7 ± 1.9 for right and left striatum, respectively, in the three subjects imaged 334 to 417 min post-tracer injection (Table 5). Ratios in later images (1085–1606 min) were higher, i.e., 9.3 ± 2.9 and 10.3 ± 3.5 for right and left striatum (Table 3). There was a focus of activity in the midline extending inferiorally (Fig. 4) from the level of the striatum designated "midbrain." The ratios of activity in this region-to-occipital cortex were 4.0 ± 1.7 and 4.1 ± 1.0 at early and later time points, respectively.

CONCLUSIONS

The present data demonstrate the radiation safety and favorable biodistribution of [^{123}I]β-CIT in humans with approximately 14% of injected dose distributing to the brain. Activity was concentrated in the striatum, a region rich in monomine transporters. Radiation-absorbed dose estimates indicate that the lungs are the limiting organ with an estimated absorbed dose of 0.1 mGy/MBq (0.38 rads/mCi).

Errors associated with the accuracy of the estimation of the organ radiation-absorbed dose in this study include the precision of the attenuation correction, the complete accounting of whole-body activity and assumptions regarding the homogeneous distribution of radioactivity within source organs.

The mean attenuation factors determined on the basis of transmission images were similar for most source organs, including brain (0.35), liver (0.31), intestine (0.30) and bladder (0.30), with the exception of lung (0.46). By assuming similar attenuation for all source organs, it is possible to forego transmission source attenuation correction and calibrate conjugate counts in all source organs to 100% injected activity. This method produces consistent overestimation of the lung-absorbed dose by approximately 50%. Additional errors of dose estimates determined without applying an attenuation correction would occur in heterogeneous subject groups. Obese individuals and female subjects (variable breast attenuation) demonstrate greater re-

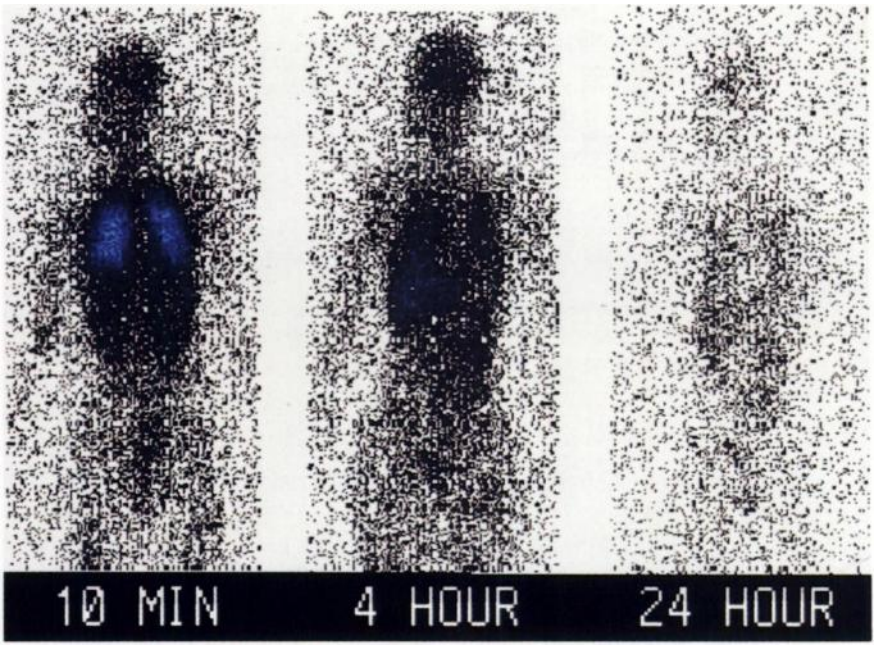

FIGURE 2. Anterior whole-body images demonstrate biodistribution of [^{123}I]β-CIT in a healthy subject 10 min, 4 hr and 24 hr postinjection.

gional differences in source organ attenuation factors. These problems suggest the utility of the regional attenuation correction using a transmission source.

Attenuation factors based on the ^{99m}Tc line source were in close agreement with attenuation correction using the ^{123}I source. The ready availability and low cost of ^{99m}Tc makes this a reasonable substitute for ^{123}I when performing transmission attenuation corrections with ^{123}I-labeled compounds. A theoretical error in calculated attenuation factors with ^{99m}Tc could arise from increased attenuation of 140 keV photons versus the slightly higher energy ^{123}I photon (159 keV). Although the mean attenuation factors calculated for both transmission correction methods were not different, there was a slight (4%–8%) increase of the

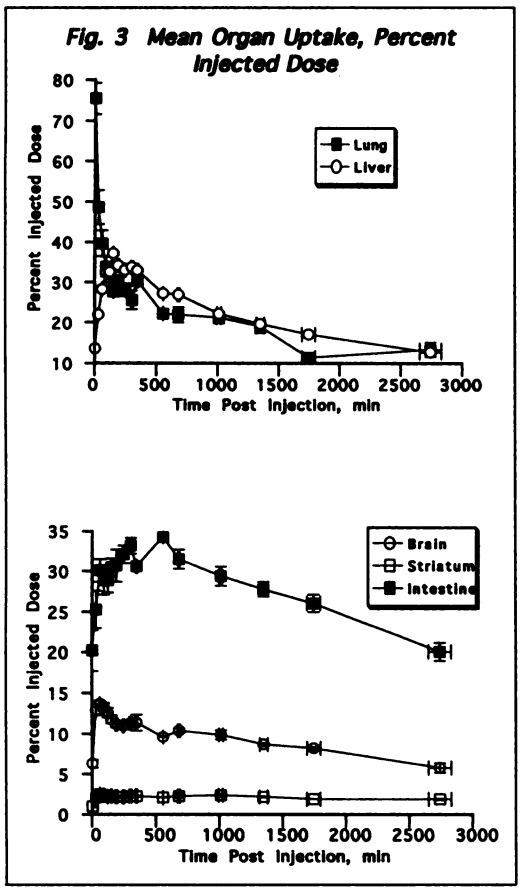

FIGURE 3. Mean organ uptakes over time in eight healthy subjects expressed as percent of injected dose of [^{123}I]β-CIT.

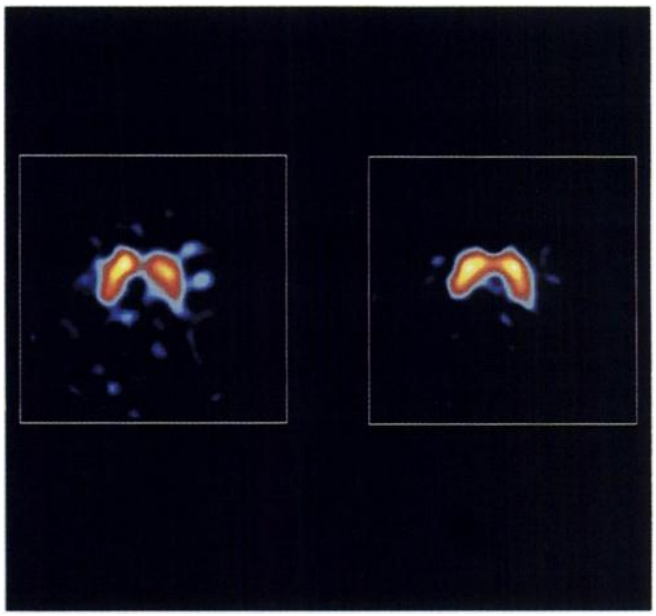

FIGURE 4. Transaxial brain SPECT images acquired at 5 and 24 hr post-[^{123}I]β-CIT injection in a healthy human subject. Images are the sum of four adjacent slices demonstrating highest striatal activity (see text for acquisition and processing data). The 5-hr image shows a midline focus of activity immediately posterior to striatum, which may represent midbrain uptake.

TABLE 3
Radiation Dose Estimates for ^{123}I β-CIT

Target organ	Estimated radiation dose (mGy/MBq)	(rads/mCi)
Lungs	0.10	0.38
Liver	0.09	0.32
Lower large intestinal wall	0.05	0.20
Upper large intestinal wall	0.05	0.18
Gallbladder wall	0.05	0.18
Brain	0.05	0.17
Urinary bladder	0.03	0.09
Small intestine	0.02	0.09
Adrenals	0.02	0.07
Heart wall	0.02	0.07
Pancreas	0.02	0.06
Bone surf	0.02	0.06
Ovaries	0.02	0.06
Kidneys	0.01	0.05
Uterus	0.01	0.04
Stomach	0.01	0.04
Thymus	0.01	0.04
Red marrow	0.01	0.04
Spleen	0.01	0.04
Breasts	0.01	0.03
Muscle	0.01	0.03
Thyroid	0.01	0.03
Testes	0.01	0.02
Skin	0.01	0.02
Effective dose	0.04	0.13

Average residence time (hr) in eight subjects	
Brain	1.59
Gallbladder contents	0.09
Lower large intestine contents	0.55
Small intestine	0.35
Upper large intestine contents	0.67
Kidneys	3.37
Liver	3.94
Lungs	3.86
Urinary bladder contents	0.24
Remainder of body	5.47

correction using ^{99m}Tc within the subjects that would increase organ radiation-absorbed dose estimates.

Recovered activity was 118%–121% of the injected activity using two different methods: summing organ ROIs and using a single whole-body ROI. Overestimation of activity with the first method may have been the result of a slight overlap in the source organ regions. The image analysis software used did not permit simultaneous display of all organ ROIs. A second possibility is an error in the factor used to convert conjugate counts to microcuries of activity based on a distributed source of ^{123}I measured in air. The introduction of a scattering medium would tend to lower the conversion factor and the recovered organ activity. To test this hypothesis, a second gauze pad containing the ^{123}I source was measured in the presence of a scattering medium. The additional scatter produced an expected decrease in the conversion factor, leading to a mean whole-body activity recovery of 108%, suggesting scatter accounts for 44% of the overestimation.

TABLE 4
Planar and SPECT Estimates of Percent Brain/Striatal Uptake*

Subject	SPECT Total brain	SPECT Striatum	Planar Total brain	Planar Striatum
A	8.2	2.7	8.1	2.2
B†	7.2	1.8	10.4	2.4
C	6.6	2.0	7.3	2.0
D	8.8	2.9	9.0	2.2

*Within subject planar and SPECT scans obtained at comparable times, expressed as percent of injected dose.

†Subject B SPECT at 334 min; whole-body SPECT at 282 min post-tracer injection.

TABLE 5
SPECT Ratio of Regional Brain Activity to Occipital Cortex*

	Time (min postinjection)	Ratio to occipital cortex: Right striatum	Left striatum	Midbrain
Early	334	2.9	3	2.2
	340	4.6	4.3	4.2
	417	7.4	6.8	5.5
Mean	363.7	5.0	4.7	4.0
s.d.	46.3	2.3	1.9	1.7
Late	1085	8.3	8.9	4.1
	1267	11.6	14.3	5.3
	1368	12.6	13.2	4.1
	1378	4.6	4.7	2.5
	1476	8.3	8.7	3.7
	1607	10.2	11.7	4.8
Mean	1363.5	9.3	10.3	4.1
s.d.	178.4	2.9	3.5	1.0

*Nine SPECT scans in eight subjects.

Normalization of whole-body recovered activity to 100% of injected activity may be used to generate time-activity data for calculating source organ residence times (τ). The error associated with this approach lies in the accurate accounting of all injected activity. For the whole-body ROI used to estimate recovery of injected activity in these data, counts present in the upper extremities distal to the elbow and the lower extremities distal to the knees were assumed to be negligible. This may be a reasonable assumption if the ROI is drawn after significant clearance of activity from the blood pool, the subject has not excreted any injected activity and there is no significant activity accumulating in regions outside the ROI. Obtaining full anterior and posterior whole images permits a more accurate assessment of injected activity for making this normalization.

The calculation of organ dose to a target organ assumes a homogeneous distribution of tracer in all irradiating source organs. This is not the case with activity distributing in brain. ROIs were drawn for the striatum on the whole-body images based on the apparent localization of activity in this area. This activity was confirmed to be in the striatum on SPECT images obtained 5.5 to 27 hr post-

radiotracer injection. Slow striatal washout of activity was demonstrated by focal brain activity on the 48-hr whole-body scans and SPECT data. The slow washout of striatal activity accounted for the relatively high striatal absorbed doses. Whole brain rather than striatum is typically used for dosimetric determination by the Medical Internal Radiation Dose Committee, although this is based on experience with tracers with a more homogeneous distribution in the brain. For stochastic radiation effects, the effective dose equivalent may be a more credible measure for determining the maximum injected dose.

These results show that the lung is the limiting organ for radiation exposure from [^{123}I]β-CIT. Based on these calculations, a dose of 500 MBq (14 mCi) of [^{123}I]β-CIT results in a mean absorbed dose of 50 mGy (5 cGy) to the lungs. The higher lung exposures are caused by a large initial uptake by the lungs driven by the large pulmonary vascular flow and a second slower-clearing component. The cause of this slower-clearing component is unknown, but it may reflect binding to monoamine transporters. Kinetic studies in two baboons did not predict these slow pulmonary clearance kinetics and relatively high absorbed doses (*11*). In these monkey studies, lower large intestine (0.2 mGy/MBq), upper large intestine (0.2 mGy/MBq), gallbladder wall (0.1 mGy/MBq), small intestine (0.07 mGy/MBq) and liver (0.05 mGy/MBq) had the highest calculated absorbed doses. The overall higher calculated absorbed doses and different rank order of the organs receiving the highest calculated absorbed doses in the baboons may be caused by species differences and the limited number of animals studied.

The SPECT images also demonstrated a focus of activity in the midline at the level of the striatum extending caudally. This was previously observed in animal studies (*11*). Based on displacement of this "midbrain" activity (but not striatal activity) with compounds that bind specifically to the serotonin transporter (*12*), the majority of this activity was thought to reflect binding to serotonin transporters. Following injection of [^{123}I]β-CIT in monkeys, ex vivo autoradiographic studies have shown high levels of activity in the superior colliculus, substantia nigra and hypothalamic nuclei (unpublished results), and these brain areas receive dense serotonergic innervation. The complete characterization of the midbrain activity in humans, both with regard to its pharmacologic specificity and anatomic localization, remains to be determined. Nonetheless, the prospect of a neurochemical imaging probe for serotonin transporters is interesting in a number neuropsychiatric disorders, including major depression, panic disorder and obsessive-compulsive disorder.

In summary, [^{123}I]β-CIT is a promising SPECT ligand for studying human central nervous system disease with favorable radiation safety, high brain uptake and localization in brain regions rich in monoamine transporters.

ACKNOWLEDGMENTS

This work was supported in part by generous gifts from Nihon Medi-Physics, Co., Ltd. (Tokyo, Japan) and Rose and Philip Hoffer, funds from the National Parkinson's Foundation, the Department of Veterans Affairs Schizophrenia Biological Research Center and NIMH (R43-MH48243). The authors thank Mr. Gary Wisniewski for expert technical support and Robert Lange, PhD for helpful comments.

REFERENCES

1. Mizukawa K, McGeer EG, McGeer PL. Autoradiographic study on dopamine uptake sites and their correlation with dopamine levels in the striata from patients with Parkinson's disease, Alzheimer disease, and neurologically normal controls. *Mol Chem Neuropathol* 1993;18:133–144.
2. Hirai M, Kitamura N, Hashumoto T, et al. [3-H]GBR-12935 binding sites in human striatal membranes: binding characteristics and changes in parkinsonians and schizophrenics. *Jpn J Pharmacol* 1988;47:237–243.
3. Janowsky A, Vocci F, Berger P, et al. [3-H]GBR-12935 binding to the dopamine transporter is decreased in the caudate nucleus in Parkinson's disease. *J Neurochem* 1987;49:617–621.
4. Reith ME, Sershen H, Lajtha A. Binding sites for [3-H]cocaine in the mouse striatum and cerebral cortex have different kinetics. *J Neurochem* 1986;46: 309–312.
5. Haberland N, Hetey L. Studies in postmortem dopamine uptake II: alterations of the synaptosomal cathecholamine uptake in postmortem brain regions in schizophrenia. *J Neural Transm* 1987;68:303–313.
6. Neumeyer JL, Wang S, Milius RA, et al. [123-I]-2-β-Carbomethoxy-3-β-(4-iodophenyl)-tropane (β-CIT): high affinity SPECT radiotracer of monamine reuptake sites in brain. *J Med Chem* 1991;34:3144–3146.
7. Innis R, Baldwin R, Sybirska E, et al. Single photon emission computed tomography imaging of monoamine reuptake sites in primate brain with [^{123}I]CIT. *Eur J Pharmacol* 1991;200:369–370.
8. Shaya EK, Scheffel U, Dannals RF, et al. In vivo imaging of dopamine reuptake sites in the primate brain using single photon emission computed tomography (SPECT) and iodine-123 labeled RTI-55. *Synapse* 1992;10:169–172.
9. Boja JW, Mitchell WM, Patel A, et al. High-affinity binding of [^{125}I]RTI-55 to dopamine and serotonin transporters in rat brain. *Synapse* 1992;12:27–36.
10. Boja JW, Patel A, Carroll FI, et al. [^{125}I]RTI-55: a potent ligand for dopamine transporters. *Eur J Pharmacol* 1991;194:133–134.
11. Baldwin RM, Zea-Ponce Y, Zoghbi SS, et al. Evaluation of the monoamine uptake site ligand [^{123}I]methyl 3β-(4-iodophenyl)tropane-2β-carboxylate ([^{123}I]β-CIT) in nonhuman primates: pharmacokinetics, biodistribution, and SPECT brain imaging coregistered with MRI. *Int J Rad Appl Instrum B* 1993;20:597–606.
12. Laruelle M, Baldwin RM, Malison RT, et al. SPECT imaging of dopamine and serotonin transporters with [^{123}I]β-CIT: pharmacological characterization of brain uptake in nonhuman primates. *Synapse* 1993;13:295–309.
13. US Pharmacopeial Convention. Sterility tests. In *The United States pharmacopeia*. Rockville, MD: United States Pharmacopeial Convention; 1990: 1483–1486.
14. Sorenson JA, Phelps ME. *Physics in nuclear medicine*. Philadelphia: WB Saunders; 1987.
15. International Commission on Radiological Protection. *Limits for intakes of radionuclides by workers*. ICRP Publication 30. New York: Pergamon Press; 1979.
16. Loevinger R, Budinger T, Watson E. *MIRD primer for absorbed dose calculations*. New York: Society of Nuclear Medicine; 1988.
17. Bøttcher J. Morphology of the basal ganglia in Parkinson's disease. *Acta Neurol Scand Suppl* 1975;62:1187.
18. Ellet W, Humes R. MIRD pamphlet no. 8: absorbed fractions for small volumes containing photon-emitting radioactivity. *J Nucl Med* 1972;7(suppl 6):25–32.